POOL BOILING OF WATER-Al_2O_3 and WATER-Cu NANOFLUIDS OUTSIDE POROUS COATED TUBES

Janusz T. Cieśliński *, Tomasz Z. Kaczmarczyk

Faculty of Mechanical Engineering

Gdansk University of Technology

Narutowicza 11/12

80 233 Gdansk, Poland

Phone: +48 58 347 16 22

Fax: +48 58 347 13 83

E-mail: jcieslin@pg.gda.pl

*) Corresponding author: E-mail: jcieslin@pg.gda.pl

ABSTRACT

This paper deals with pool boiling of water-Al_2O_3 and water-Cu nanofluids on porous coated, horizontal tubes. Commercially available stainless steel tubes having 10 mm OD and 0.6 mm wall thickness were used to fabricate test heater. Aluminium porous coatings of 0.15 mm thick with porosity of about 40% were produced by plasma spraying. Smooth tube served as a reference tube. The experiments were conducted under different absolute operating pressures, i.e. 200 kPa, 100 kPa and 10 kPa. Nanoparticles were tested at the concentration of 0.01%, 0.1%, and 1% by weight.

In all cases tested enhancement heat transfer was always observed during boiling of water-Al_2O_3 and water-Cu nanofluids on smooth tubes compared to boiling of distilled water. Contrary to smooth tubes addition of even small amount of nanoparticles resulted in deterioration of heat transfer during pool boiling of water-Al_2O_3 and water-Cu nanofluids on porous coated tube in comparison with boiling of distilled water.

INTRODUCTION

Development of methods to increase boiling heat transfer coefficients, critical heat fluxes and, where it is desirable to obtain the highest heat flux by applying the smallest wall superheat is of primary importance in many practical applications. The goal may be to reduce the heat exchanger size or pumping power required for a specified heat duty, and also to prevent excessive temperature, or even system destruction, in systems where heat generation rates are fixed – for instance in nuclear fuel assemblies or in chemical reactors.

There are two main possibilities of nucleate pool boiling heat transfer intensification. First, it is improving nucleation ability of the heat transfer surface by increasing the number of active nucleation sites and as a result one obtains so called enhanced boiling

surfaces [1-3]. It is well known that one of the most efficient category of enhanced boiling surfaces are porous coated surfaces [4].

Second, one can change thermophysical properties of the boiling liquid, for instance its surface tension by chemical additives [5,6]. Quite new possibility gives addition of small amount of nanoparticles to the base liquid obtaining nanofluid [7-9]. Comprehensive reviews on heat transfer augmentation with nanofluids have been offered by Wang and Mujumdar [10], Godson et al. [11] and Barber et al. [12].

Contrary statements about nanoparticle influence on nucleate pool boiling heat transfer on smooth and rough surfaces can be found in the literature [13]. Some papers report no change of heat transfer, some present deterioration and some heat transfer enhancement. Significant CHF enhancement occurs with various nanoparticle materials at relatively low concentrations [14]. The final enhancement depends on many factors, such as concentration of nanoparticles, nanoparticle material, nanoparticle mean diameter and size distribution, ratio of roughness height to nanoparticle diameter [15] and stability of nanofluid [16]. Recently, Kathiravan et al. [17] and Ahmed and Hamed [18] have shown that both the acidity and method of preparation of nanofluid have significant effect on nucleate pool boiling heat transfer on smooth surfaces.

Very limited data is available in the open literature regarding boiling of nanofluids on enhanced surfaces. Liu et al. [19] studied pool boiling of water–CuO nanofluid of several nanoparticle concentrations from 0.1% to 2% by weight on horizontal copper plate with microgrooves. The grooves were of 0.5 mm wide and of 0.8 mm deep. The gap between the two grooves was 0.5 mm. The experiments were conducted under four operating pressures of 7.4 kPa, 20 kPa, 31.2 kPa and 100 kPa. Independent of operating pressure significant heat transfer enhancement was observed for nanoparticle concentrations lower than 1%. For nanoparticle concentrations above 1% heat transfer deterioration was

recorded. For optimum nanoparticle concentration of 1% and operating pressure of 7.4 kPa heat transfer coefficient for nanofluid was about two times higher than for pure water.

Yang and Liu [20] carried out experiments with boiling of R141b-Au nanofluids on horizontal structured and porous coated tubes with outside diameter from 18 to 19.5 mm. The concentration of nanoparticles was 0.09% and 0.4% by volume. For structured tube, with so called re-entrant cavities, results obtained for refrigerant R141b-Au nanofluids - independent of nanoparticle concentration, overlap with that for a pure refrigerant. For porous coated tube and heat flux below 35 kW/m^2, higher heat transfer coefficient was obtained for pure refrigerant – independent of nanoparticle concentration. For heat flux above 35 kW/m^2 and lower nanoparticle concentration, i.e. 0.09%, higher heat transfer coefficient was obtained for R141b-Au nanofluid.

The main aim of the present investigation was to obtain boiling characteristics, i.e. boiling curves, heat transfer coefficients and enhancement factors for water-Al_2O_3 and water-Cu nanofluids while boiling them on horizontal, smooth and porous coated tubes under different absolute operating pressures, i.e. 200 kPa, 100 kPa and 10 kPa for three nanoparticle concentrations, i.e. of 0.01%, 0.1%, and 1% by weight.

EXPERIMENTAL SETUP AND PROCEDURE

Figure 1 shows a schematic diagram of the experimental apparatus. The test chamber consisted of a cubical vessel made of stainless steel with inside dimensions of 150 mm x 150 mm x 250 mm. Well insulated test chamber was equipped with three inspection windows for direct observation of the boiling process. The fluid temperature t_f was measured by use of six K-type thermocouples with an accuracy of ±0.1 °C. The thermocouples recorded fluid temperature at three different levels. Inside the test chamber was mounted a condenser supplied with a tap water used as a coolant. The

pressure in the test chamber was controlled by variation of the mass flow rate of cooling water flowing through the condenser. The pressure in the test chamber was measured by use of Bourdon type manometer which is accurate to ±0.25%. More details of the experimental setup are presented in [21].

Heating section

Commercially available stainless steel tubes having 10 mm OD and 0.6 mm wall thickness were used to fabricate test heater. The effective length of a tube was 100 mm. A resistance cartridge heater with diameter of 6.5 mm was inserted into the test tube to generate heat flux from an electrical power supply. The power supply can be adjusted by an electrical transformer. The final design of present heating section has been established after many practical trials supported by numerical simulations of 3D temperature fields [22].

Great care must be exercised with the cartridge heater and temperature measuring instrumentation to ensure good accuracy of the measurement of the inside temperature of the heating cylinder [23]. In present study inside the stainless steel tube a copper sleeve with four grooves (0.5x0.5 mm) at the outside surface to locate the thermocouples was inserted. Twelve K-type thermocouples installed in the grooves were used to measure inside temperature of the tube. The hot ends of the thermocouples were fixed in the middle of the Teflon rings separating cartridge heater from the wall of the tube – Figure 2. In order to ensure good heat transmission between cartridge heater and the wall of the tube thermally conductive compound Arctic Silver was used. The maximum variation in the 12 thermocouples readings was 3.5K. The detailed geometry of the test tube is shown in Figure 2.

Reference tube surface was polished with abrasive compound, so the surface roughness was estimated as R_a=0.06 μm by use of PGM-1 surface analyzer. In order to ensure consistent surface state after each test, the boiling surface was prepared in the same manner, i.e., the stainless steel tube was finished with emery paper 400, next was polished with abrasive compound, then the test tube was placed in an ultrasonic washer for 1 h. Finally, the boiling surface was cleaned by water jet.

Aluminium porous coatings of 0.15 mm thick with porosity of about 40% were produced by plasma spraying. The pore size distribution was determined by metallographic scanning. For that aim Super Vist and Svistmet systems were used. A sufficient number of image fields were analyzed so that a statistically reliable result was obtained. The mean pore radius was estimated as equal to 2.8 μm. Figure 3 shows the image of the metallographic specimen of the metallic porous coating.

Tested nanofluids

In this study Al_2O_3 and copper nanoparticles were used while distilled, deionized water was applied as a base fluid. Nanofluids with different concentrations were prepared for the experiments. Nanoparticles of the required amount and base liquid were mixed together. Ultrasonic vibration was used for 4 h in order to stabilise the dispersion of the nanoparticles. Alumina (Al_2O_3) and copper nanoparticles were tested at the concentration of 0.01%, 0.1%, and 1% by weight. Alumina nanoparticles, of spherical form have diameter from 5 nm to 250 nm; their mean diameter was estimated to be 47 nm according to the manufacturer (Sigma-Aldrich Co.). Copper nanoparticles, of spherical form have diameter from 7 nm to 257 nm; their mean diameter was estimated to be 48 nm according to the manufacturer (Sigma-Aldrich Co.). The measured pH values for Al_2O_3 nanofluids with nanoparticle concentration of 0.01%, 0.1% and 1% were 6.51,

7.48, and 8.11, respectively. The measured pH values for Cu nanofluids with nanoparticle concentration of 0.01%, 0.1% and 1% were 7.44, 6.30, and 6.87, respectively. The stability of the produced nanofluids was pretty good, which can stay for a few days without visually observable sedimentation. As an example Fig. 4 shows images of the tested water-Al_2O_3 nanofluid with nanoparticle concentration of 0.01% just after fabrication – Fig. 4a and after the experiment – Fig. 4b.

Experimental procedure

The liquid level was maintained at about 15 mm above the centerline of the test tube. In a typical experiment, before the test begins, a vacuum pump was used to evacuate the accumulated air from the vessel. Nanofluid at a preset concentration was charged and then preheated to the saturated temperature by auxiliary heater. Next the cartridge heater was switched on. The measurement was first performed at the lowest power input. Data were collected by increasing the heat flux by small increments. At each level of heat input (heat flux) equilibrium was established before taking data. It generally took about 20 min to achieve steady conditions after the power level was changed. So, the time period of single run was about 3 hours. Experiments were performed for three values of absolute pressure in the test chamber, i.e. 200 kPa, 100 kPa and 10 kPa.

Before each test, the test chamber was thoroughly washed using distilled water. A preliminary test was conducted using distilled water to verify that the experimental vessel was not contaminated by nanoparticles from the previous test.

Data reduction and uncertainty estimation

Heat flux was calculated as

$$q = \frac{UI}{\pi D_o L} = \frac{N}{\pi D_o L} \tag{1}$$

The wall temperature of a base tube t_w was calculated from the formula [24]

$$t_w = t_i - UI\frac{\ln(D_o / D_i)}{2\pi\lambda L} \tag{2}$$

where t_i was calculated as the arithmetic mean of twelve measured inside wall temperatures

$$t_i = \frac{\sum_{i=1}^{i=12} t_{i,loc}}{12} \tag{3}$$

Wall superheat was estimated as

$$\Delta T = t_w - t_f \tag{4}$$

where t_f was calculated as the arithmetic mean of six measured fluid temperatures (Figure 1)

$$t_f = \frac{\sum_{i=1}^{i=6} t_{f,loc}}{6} \tag{5}$$

Mean heat transfer coefficient was calculated as

$$\alpha = \frac{q}{\Delta T} \tag{6}$$

The uncertainties of the measured and calculated parameters are estimated by mean-square method. The experimental uncertainty of heat flux was estimated as follows:

$$\Delta q = \sqrt{\left(\frac{\partial q}{\partial N}\Delta N\right)^2 + \left(\frac{\partial q}{\partial D_o}\Delta D_o\right)^2 + \left(\frac{\partial q}{\partial L}\Delta L\right)^2} \tag{7}$$

Where the absolute measurement errors of the electrical power ΔN, outside tube diameter ΔD_o and active length of a tube ΔL are 10 W, 0.02 mm, and 1 mm, respectively. So, the maximum overall experimental limits of error for heat flux extended from ±1.3% for maximum heat flux up to ±6.5% for minimum heat flux.

The experimental uncertainty for the average heat transfer coefficient is calculated as

$$\Delta\alpha = \sqrt{\left(\frac{\partial\alpha}{\partial q}\Delta q\right)^2 + \left(\frac{\partial\alpha}{\partial\Delta T}\delta T\right)^2} \tag{8}$$

where the absolute measurement error of the wall superheat, δT, estimated from the systematic error analysis [21] equals ±0.2 K. The maximum error for average heat transfer coefficient was estimated to ±9.6%.

RESULTS

In order to validate the apparatus as well as experimental procedure, the present data obtained on a smooth horizontal stainless steel tube for distilled water were compared with those predicted by Cooper [25]

$$\alpha = 55\mathrm{P}_r^{0.12-0.434\left(\log R_p\right)}\left[-0.434\left(\log P_r\right)\right]^{-0.55} M^{-0.5}\left(q_w\right)^{0.67} \tag{9}$$

and Cornwell-Houston [26] correlations

$$Nu = 9.7P_{cr}^{0.5}F(A_p)\,\mathrm{Re}^{0.67}\,\mathrm{Pr}^{0.4} \tag{10}$$

with

$$F(P) = 1.8P_r^{0.17} + 4P_r^{1.2} + 10P_r^{10} \tag{11}$$

where $P_r=P/P_{cr}$. Surface roughness parameter R_p in Eq. 9 was assumed to be equal R_a. Figure 5 shows comparison of present experimental data with predictions made by Eqn. (9) an (10) taking heat flux as abscissa and heat transfer coefficient as ordinate. Present data for the boiling of distilled water are found to be in reasonable agreement with those predicted by Cooper correlation (within a band error ±4.5%) while Cornwell-Houston correlation overpredicts obtained results, particularly for higher heat fluxes.

Figure 6, in turn, shows comparison of present data for water-Al_2O_3 nanofluid with 1% (by weight) nanoparticle concentration and data obtained by Das et. al [27] and Wen and Ding [28]. Originally given by Das et al. nanoparticle concentration by volume (0.1%) was recalculated by use of formula proposed by Bang and Chang [29]

$$\Phi_V = \frac{1}{\left(\frac{1-\Phi_m}{\Phi_m}\right)\frac{\rho_p}{\rho_{bf}}+1} \tag{12}$$

Finally, it was estimated that 0.1% Al_2O_3 nanoparticle concentration by volume in distilled water corresponds to 0.4% nanoparticle concentration by weight.

Contrary to Das et al. study - where deterioration of heat transfer was observed with boiling of water-Al_2O_3 nanofluid on smooth tube, present data show heat transfer enhancement. This contradictory behaviour may result from various nanoparticle concentration in both studies as well as different heating surface roughness. Wen and Ding [28] data show reasonable agreement with present data, although were obtained for different heater geometry, i.e. a stainless steel disc with diameter of 150 mm.

As an example Figure 7 and Figure 8 show boiling curves for water-Al_2O_3 and water-Cu nanofluids on smooth stainless steel tube at subatmospheric pressure (10 kPa) for three tested nanoparticle concentrations, i.e. 0.01%, 0.1%, and 1%. It is seen in Fig. 7 and Fig. 8 that addition of even small amount of nanoparticles results in heat transfer enhancement - boiling curves are shifted left, towards lower wall superheats. Additionally, independent of operating pressure, sub- and atmospheric pressure, and overpressure, increase of nanoparticle concentration results in heat transfer coefficient enhancement.

Figure 9 and Figure 10 display boiling curves for water-Al_2O_3 and water-Cu nanofluids on porous coated tube at sub-atmospheric pressure (10 kPa) for three tested nanoparticle concentrations, i.e. 0.01%, 0.1%, and 1%. Contrary to smooth tubes (Fig. 7 and Fig. 8) addition of nanoparticles inhibits heat transfer in comparison with boiling of distilled water - boiling curves are shifted right, towards higher wall superheats. Moreover, for both nanofluids tested maximum deterioration of heat transfer performance was recorded for highest nanoparticle concentration, i.e. 1%.

Figure 11 shows heat transfer coefficient during boiling of water-Al_2O_3 nanofluid with 1% nanoparticle concentration on porous coated tube at different operating pressures. Increase of pressure evidently results in heat transfer coefficient increase.

Figure 12 shows heat transfer coefficient during boiling of water-Cu nanofluid with 0.1% nanoparticle concentration on porous coated tube at different pressures. Similarly as for water-Al_2O_3 nanofluid boiling, increase of operating pressure results in heat transfer enhancement.

Figure 13 displays effect of operating pressure on enhancement factor k_{eff} – defined as a ratio of the heat transfer coefficient for nanofluid to the heat transfer coefficient for distilled water at the same wall superheat, during boiling of water-Al_2O_3 nanofluid on porous coated tube and tested nanoparticle concentrations, i.e. 0.01%, 0.1% and 1%. As it is seen in Figure 13, independent of nanoparticle concentration and operating pressure value of the enhancement factor is below one – it means that for given heat flux, heat transfer coefficient for distilled water is higher than for nanofluid while boiling on the tested porous coated tube. Additionally, enhancement factor increases, particularly for overpressure, with heat flux increase.

Figure 14 and Figure 15 illustrate, in turn, enhancement factor k_{eff}, during boiling of water-Al_2O_3 nanofluid on smooth stainless steel and porous coated tube at atmospheric pressure against nanoparticle concentration, respectively. Contrary to porous coated tube, significant increase of the enhancement factor k_{eff} has been recorded for smooth stainless steel tube with heat flux decrease. For porous coated tube the enhancement factor does not depend on heat flux and slightly decreases with nanoparticle increase from 0.1% to 1%.

Figure 16 illustrates the effect of porous coating on heat transfer performance during boiling of distilled water and examined nanofluids with the same nanoparticle

concentration, i.e. 0.1% at overpressure in the test chamber (200 kPa). It is seen in Figure 16 that application of porous coating results in distinct enhancement of heat transfer coefficient during boiling of distilled water although enhancement ratio slightly decreases with heat flux increase. Application of porous coating during boiling of nanofluids depends on nanoparticle material. For water-Cu nanofluid enhancement ratio is above 1 and is almost independent of heat flux. This means that application of porous coating during boiling of water-Cu nanofluid benefits in heat transfer enhancement. Contrary to water-Cu nanofluid use of water-Al_2O_3 nanofluid exhibits distinct deterioration of heat transfer coefficient on porous coated tube, but enhancement ratio increases with heat flux increase.

Correlation

A multidimensional regression analysis using the least squares method was used to establish correlation equation for prediction of an average heat transfer coefficient during pool boiling of water-Al_2O_3 and water-Cu nanofluids of different nanoparticle concentration on horizontal porous coated tube at various operating pressures

$$Nu = 112 C_{sf} Bo^{0.197} \left(\frac{P}{P_{cr}} \right)^{0.0182} \left(\frac{a}{D_p} \right)^{0.03} \left[(1 - \ln \Phi)^{\Phi} \right]^{-0.18} \tag{13}$$

Proposed correlation includes all tested variables in dimensionless form, i.e.: nanoparticle concentration (in weight per cent), ratio of the surface state parameter to nanoparticle diameter, where surface state parameter is assumed to be a mean pore radius of porous coatings, reduced pressure, boiling number, and surface/liquid parameter. The surface/liquid parameter estimated using regression analysis was equal to C_{sf} = 0.759 for both water-Al_2O_3 and water-Cu nanofluids.

A comparison of the predicted data against the experimentally obtained under the present investigation is displayed in Figure 17. For about 97% of experimental points the discrepancy between experimental data and values calculated from the proposed correlation is lower than ±25%.

Versatility of the proposed correlation was checked by recalculation of the Das et al. [27] data for smooth surface and Yang and Liu [20] results for porous coated tube by use of Eq. 13. Figure 18 shows comparison of the experimental data obtained by Das et al. [27] for water-Al_2O_3 nanofluid and predictions made by use of present correlation. Reasonable agreement has been obtained although present correlation overpredicts and underpredicts Das et al. data for lower and higher heat fluxes, respectively.

Figure 19 shows comparison of the experimental data obtained by Yang and Liu [20] for R141b-Au nanofluid boiling on porous coated tube and predictions made by use of present correlation. Assuming surface/liquid parameter C_{sf}=1.2 - with the same other constants (exponents) in Eq. 13, present correlation reproduces Yang and Liu data quite reasonable. Because of the lack of the thermophysical properties of the R141b-Au nanofluid necessary data were taken as for pure R141b.

Discussion

The potential explanation of the heat transfer degradation during nanofluid boiling on porous coated surface is reduction of the number of active nucleation sites because of nanoparticles trapping inside a porous matrix – Fig. 20. In some places concentration of the nanoparticles can be so big that the pore becomes inactive. And what is the mechanism of nanoparticles inflow into the porous structure? We should remember that nucleate boiling is a very dynamic process [30]. So, during the bubble growth period and just after bubble departure the pressure inside a porous matrix drops substantially. It triggers liquid – in this case with dispersed nanoparticles, inflow from the pool into the

porous layer. This mechanism (called suction-evaporation) probably explains the increase of heat transfer coefficient of nanofluids with heat flux increase during boiling on porous surfaces, too. With heat flux increase pressure fluctuations inside a porous layer increase too. So, for higher heat flux values it is possible that, because of strong pressure fluctuations, pores clogged by nanoparticles can be re-opened and serve as active nucleation sites.

CONCLUSIONS

- Independent of operating pressure addition of even small amount of Al_2O_3 or Cu nanoparticles inhibits heat transfer during boiling of water-Al_2O_3 and water-Cu nanofluids on porous coated horizontal tubes in comparison with boiling of distilled water.
- Heat transfer coefficient decreases with nanoparticle concentration increase.
- Independent of concentration, increase of pressure results in heat transfer coefficient increase.
- Heat transfer coefficients predicted by use of the proposed Nusselt-type relation correlate satisfactory with the experimental data related to the tested nanofluids over some range of nanoparticle concentration and operating pressure.
- Present rough correlation reproduces quite reasonable published data with adjusting only one factor, i.e. surface/liquid parameter C_{sf}. More general form of the proposed correlation should include additional parameters of the porous coating, first of all the porosity. So, more experimental data are needed on well defined porous coatings and various surface/liquid combinations.

ACKNOWLEDGEMENT

This work was sponsored by the Ministry of Research and Higher Education, Grant No. N N512 374435.

NOMENCLATURE

a – mean pore radius (m)

Bo – boiling number, $Bo = \frac{qS\rho_l}{\rho_v h_{fg} \mu_l}$

C_{sf} - surface/liquid parameter in Eq. (13)

D - diameter (m)

h_{fg} – latent heat of vaporization (kJ/kg)

I – current (A)

L - active length of the tube (m)

M – molecular weight (kg/kmol)

N - electrical power (W)

Nu – Nusselt number $Nu = \frac{\alpha D_t}{\lambda_l}$

P – pressure (kPa)

S – constant $S = \sqrt{\frac{\sigma}{g(\rho_l - \rho_v)}}$

T - temperature (K)

U – voltage (V)

q – heat flux (W/m^2)

Greek symbols

α average heat transfer coefficient (W/m^2K)

λ thermal conductivity (W/mK)

ρ density (kg/m^3)

σ surface tension coefficient (N/m)

Φ concentration of nanoparticles by weight (%)

μ dynamic viscosity (Pas)

Subscripts

bf – base fluid

f – fluid

cr – critical

l – liquid

i – inside

loc – local

m - mass

o – outside

p – particle

pc – porous coating

s - smooth

r – reduced

v – vapor

vol - volume

w - wall

REFERENCES

[1] Thome, J. R., *Enhanced boiling heat transfer*, Hemisphere, NY, 1990.

[2] Bergles, A.E., ExHFT for fourth generation heat transfer technology, *Experimental Thermal and Fluid Science*, vol. 26, pp. 335-344, 2002.

[3] Webb, R.L., Odyssey of the enhanced boiling surface, *Transactions of the ASME J. Heat Transfer*, vol. 126, pp. 1051-1059, 2004.

[4] Cieśliński, J.T., Flow and Pool Boiling on Porous Coated Surfaces, *Rev Chem Eng*, vol. 27, pp. 179-190, 2011.

[5] Hetsroni, G., Gurevich, M., Mosyak, A., Rozenblit, R., and Segal, Z., Boiling enhancement with environmentally acceptable surfactants, *Int. J. Heat and Fluid Flow*, vol. 25, pp. 841–848, 2004.

[6] Cheng, L., Mewes, D., and Luke, A, Boiling phenomena with surfactants and polymeric additives: A state-of-the-art review. *Int. J. Heat and Mass Transfer*, vol. 50, pp. 2744–2771, 2007.

[7] Choi, S., Enhancing thermal conductivity of fluids with nanoparticles, Developments and Applications of Non-Newtonian Flows, ASME, FED-vol. 231/MD-vol. 66, 99-105, 1995.

[8] Das, S.K, Choi, S.U.S., and Patel, H.E., Heat Transfer in Nanofluids — A Review, *Heat Transfer Engineering*, vol. 27, Issue 10, pp. 3–19, 2006.

[9] Choi, S.U.S., Nanofluids: A New Field of Scientific Research and Innovative Applications, *Heat Transfer Engineering*, vol. 29, Issue 5, pp. 429-431, 2008.

[10] Wang, X.Q., and Mujumdar, A.S., Heat transfer enhancement of nanofluids: a review. *Int. J. Thermal Sc*., vol. 46, pp. 1-9, 2007.

[11] Godson, L., Raja, B., Lal, D.M., and Wongwises, S., Enhancement of heat transfer using nanofluids – An overview. *Renewable and Sustainable Energy Reviews*, vol. 14, pp. 629-641, 2010.

[12] Barber, J., Brutin, D., and Tadrist, L., A review on boiling heat transfer enhancement with nanofluids. *Nanoscale Research Letters*, 6:280, 2011.

[13] Cieśliński, J.T., and Kaczmarczyk, T.Z,, Pool boiling of water-Al_2O_3 and water-Cu nanofluids on horizontal smooth tubes. *Nanoscale Research Letters*, doi:10.1186/1556-276X-6-220, 2011.

[14] Kim, H., Enhancement of critical heat flux in nucleate boiling of nanofluids: a state-of-art review. *Nanoscale Research Letters* 2011, 6:415 doi:10.1186/1556-276X-6-415, 2011.

[15] Narayan, G. P., Anoop, K. B., and Das, S. K., Mechanism of enhancement/deterioration of boiling heat transfer using stable nanoparticle suspensions over vertical tubes, *J. Applied Physics*, vol. 102, pp. 074317, 2007.

[16] Yang, X., and Liu, Z., A Kind of Nanofluid Consisting of Surface-Functionalized Nanoparticles, *Nanoscale Research Letters*, vol. 5, pp. 1324–1328, 2010.

[17] Kathiravan, R., Kumar, R., Gupta, A., and Chandra R., Preparation and Pool Boiling Characteristics of Silver Nanofluids Over a Flat Plate Heater, *Heat Transfer Engineering*, vol. 33, Issue 2, pp. 69-78, 2012.

[18] Ahmed, O, and Hamed, M.S., Effects of Acidity and Method of Preparation on Nucleate Pool Boiling of Nanofluids, *Heat Transfer Engineering*, vol. 33, Issue 14, pp. 1148-1153, 2012.

[19] Liu, Z., Xiong, J., and Bao, R., Boiling heat transfer characteristics of nanofluids in a flat heat pipe evaporator with micro-grooved heating surface, *Int. J. Multiphase Flow*, vol. 33, pp. 1284-1295, 2007.

[20] Yang, Ch., and Liu, Da., Pool boiling on plain and enhanced tubes of refrigerant R141b with nanoparticles, *Proc. of 5th Int. Conf. On Multiphase Flow*, ICMF'2004, Yokohama, Paper No. 365, 2004.

[21] Kaczmarczyk, T.Z., Boiling of nanofluids on horizontal tubes with modified surface. PhD thesis, Gdansk University of Technology, Poland, 2012.

[22] Cieśliński, J.T., Krasowski, K., and Kaczmarczyk, T.Z., Simulation of temperature field in cylindrical boiling heating section. *Turbulence: International Journal*, vol. 12, pp. 59 – 64, 2007.

[23] Marto, P. J., and Anderson, C. L., Nucleate boiling characteristics of R-113 in small tube bundle, *Transactions ASME J. Heat Transfer*, Vol. 114, pp. 425-433, 1992.

[24] Chiou, Ch.B., Lu, D.Ch., and Wang, Ch.Ch., Pool boiling of R-22, R124 and R-134a on a plain tube, *Int. J. Heat Mass Transfer*, Vol. 40, pp. 1657-1666, 1997.

[25] Cooper, M.G.: Heat Flow in Saturated Nucleate Pool Boiling – A Wide-Ranging Examination Using Reduced Properties. *Advances in Heat Transfer*, vol. 16, 1984, 157-239.

[26] Cornwell, K., Houston, S.D: Nucleate pool boiling on horizontal tubes: a convection-based correlation. *Int. J. Heat Mass Transfer*, vol. 37, pp. 303-309, 1994.

[27] Das, S.K., Putra, N., Roetzel, W.: Pool boiling characteristics of nano-fluids. *Int. J. Heat and Mass Transfer*, vol. 47, pp. 851-862, 2003.

[28] Wen, D., Ding, Y.: Experimental investigation into the boiling heat transfer of aqueous based γ-alumina nanofluids. *J. Nanoparticles Research*, vol. 7, pp. 265-274, 2005.

[29] Bang, I.C., Chang, S.H.: Boiling heat transfer performance and phenomena of Al_2O_3 – water nano-fluids from a plain surface in a pool. *Int. J. Heat and Mass Transfer*, vol. 48, pp. 2407-2419, 2005.

[30] Nakayama, W., Daikoku, T., and Nakajima, T., Effects of pore diameter and system pressure on saturated pool boiling heat transfer from porous coated surfaces. *Transactions ASME J. Heat Transfer*, vol. 104, pp. 425-433, 1982.

Figure captions

Figure 1 Scheme of the experimental rig: 1 – heating section, 2 – experimental vessel, 3 – inspection windows, 4 – condenser, 5 – insulation, 6 – safety-valve, 7 – manometer, 8 – rotameter, 9 – autotransformer, 10 – ammeter, 11 – millivoltmeter, 12 – switch, 13 – voltmeter, 14 – ice-point, 15 – auxiliary heater, 16 – autotransformer, 17 – ultrasonic washer, T – thermoelement, ZS – drain valve, ZR – control valve, ZO – cut-off valve, ZB – safety-valve.

Figure 2 Details of the test section; 1- heating surface, 2 – cartridge heater, 3 – Teflon ring, 4 – copper sleeve, 5 – thermocouples, 6 – insulating cap

Figure 3 Image of the metallographic specimen of the coating.

Figure 4 SEM images of the water-Al_2O_3 nanofluid; a) fresh, b) after experiment

Figure 5 Variation of present results with Cooper [25] and Cornwell-Houston correlations

Figure 6 Comparison of present experimental results with data obtained by Das et. al [27] and Wen and Ding [28] for water-Al_2O_3 nanofluid

Figure 7 Boiling curves for water-Al_2O_3 nanofluid on smooth stainless steel tube at subatmospheric pressure (10 kPa)

Figure 8 Boiling curves for water-Cu nanofluid on smooth stainless steel tube at subatmospheric pressure (10 kPa)

Figure 9 Boiling curves for water-Al_2O_3 nanofluid on porous coated tube at subatmospheric pressure (10 kPa)

Figure 10 Boiling curves for water-Cu nanofluid on porous coated tube at subatmospheric pressure (10 kPa)

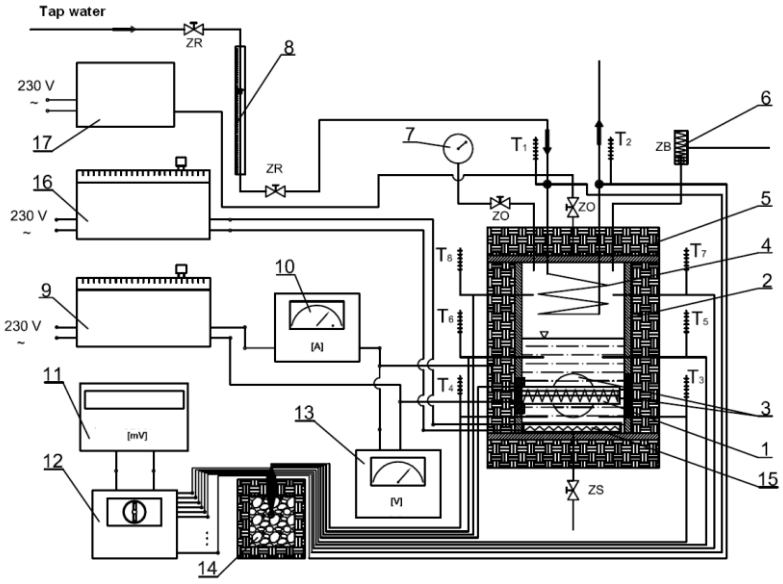

Figure 1 Scheme of the experimental rig: 1 – heating section, 2 – experimental vessel, 3 – inspection windows, 4 – condenser, 5 – insulation, 6 – safety-valve, 7 – manometer, 8 – rotameter, 9 – autotransformer, 10 – ammeter, 11 – millivoltmeter, 12 – switch, 13 – voltmeter, 14 – ice-point, 15 – auxiliary heater, 16 – autotransformer, 17 – ultrasonic washer, T – thermoelement, ZS – drain valve, ZR – control valve, ZO – cut-off valve, ZB – safety-valve

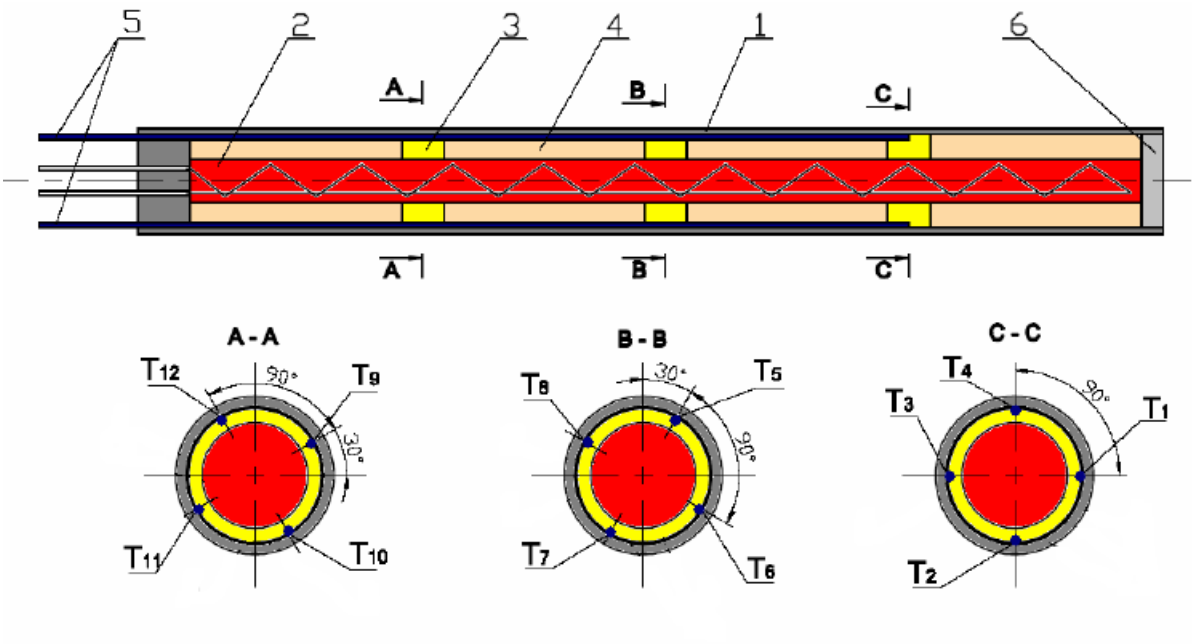

Figure 2 Details of the test section; 1- heating surface, 2 – cartridge heater, 3 – Teflon ring, 4 – copper sleeve, 5 – thermocouples, 6 – insulating cap

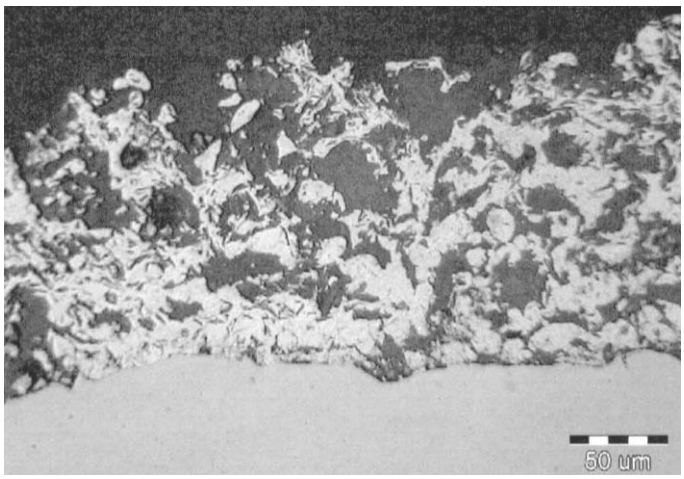

Figure 3 Image of the metallographic specimen of the porous coating

a) b)

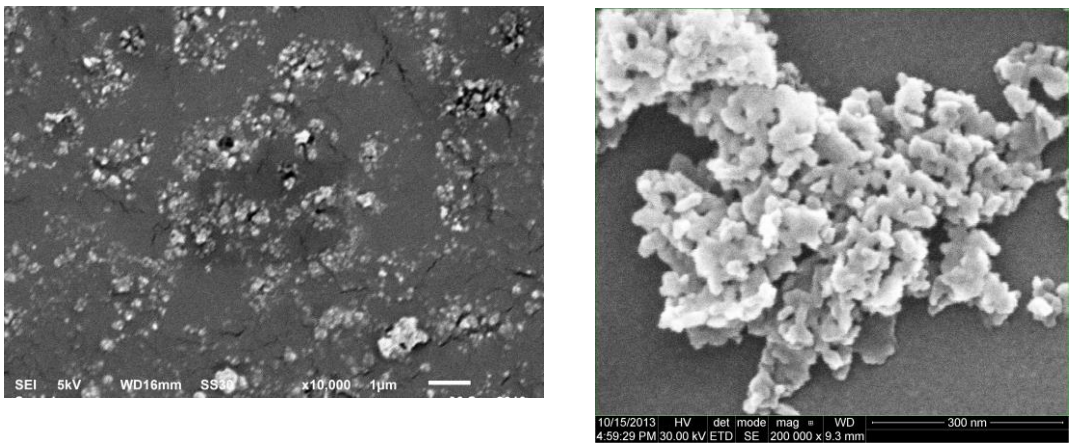

Figure 4 SEM images of the water-Al_2O_3 nanofluid; a) fresh, b) after experiment

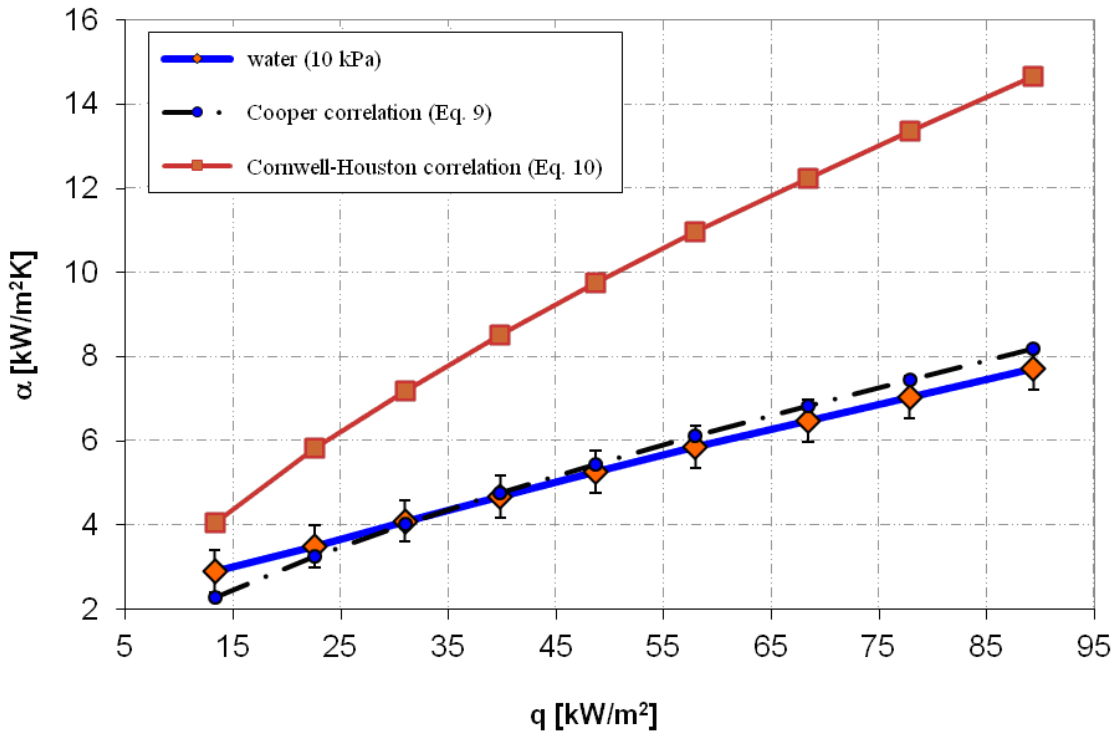

Figure 5 Variation of present results with Cooper [25] and Cornwell-Houston [26] correlations

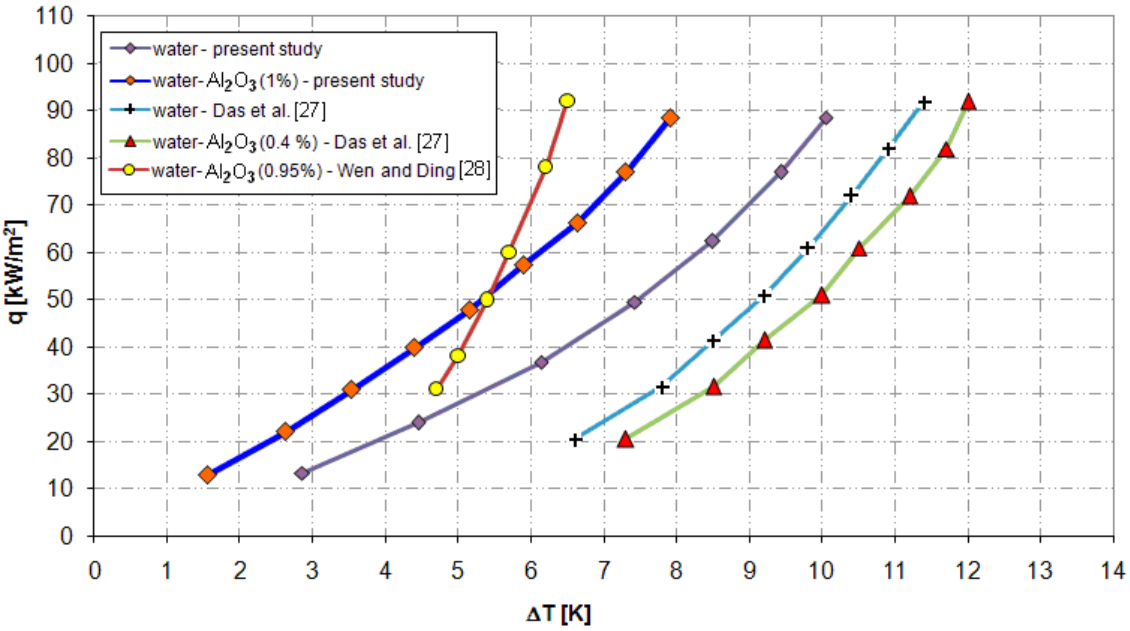

Figure 6 Comparison of present experimental results with data obtained by Das et al. [27] and Wen and Ding [28] for water-Al_2O_3 nanofluid

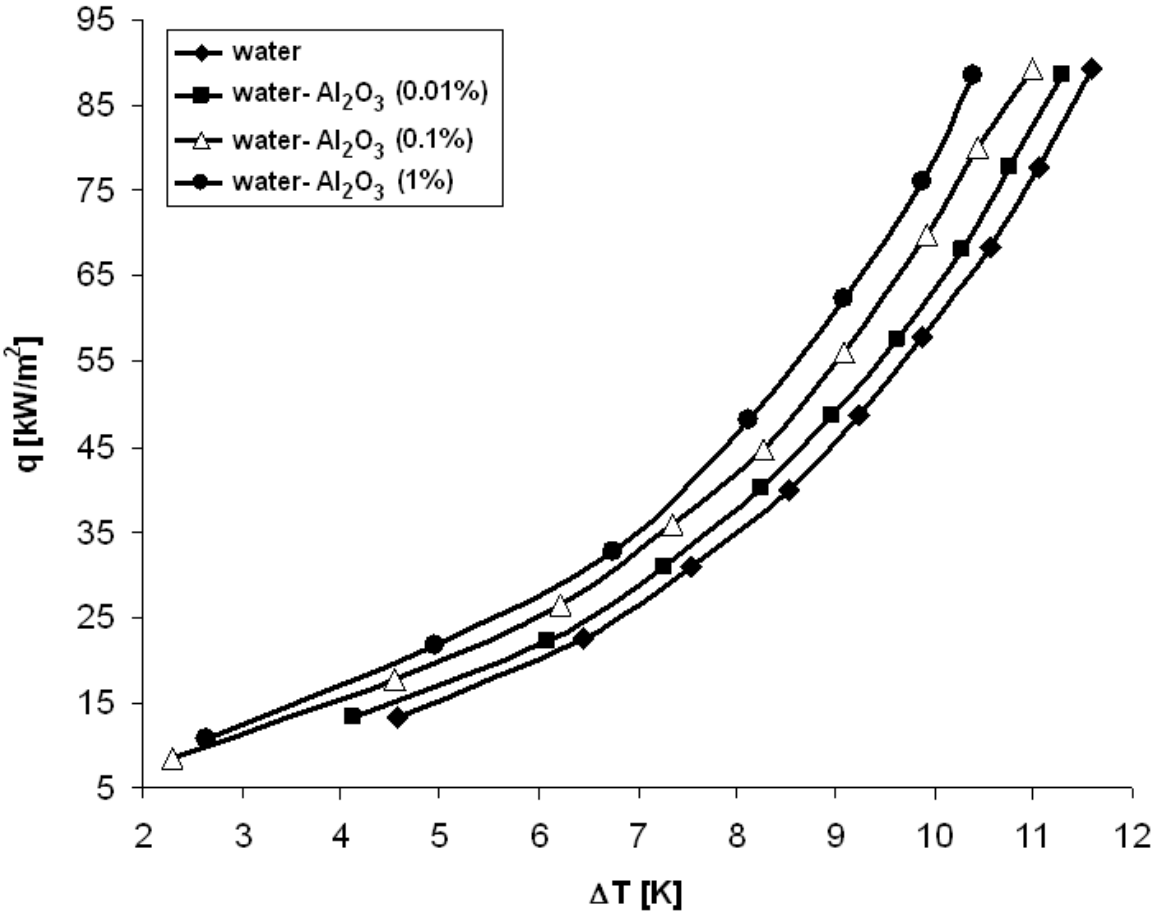

Figure 7 Boiling curves for water-Al_2O_3 nanofluid on smooth stainless steel tube at subatmospheric pressure (10 kPa)

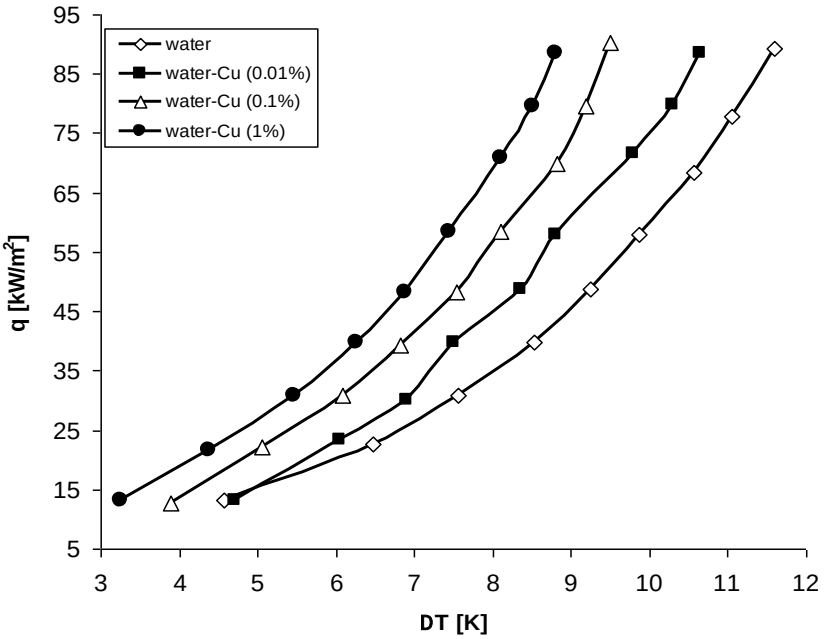

Figure 8 Boiling curves for water-Cu nanofluid on smooth stainless steel tube at subatmospheric pressure (10 kPa)

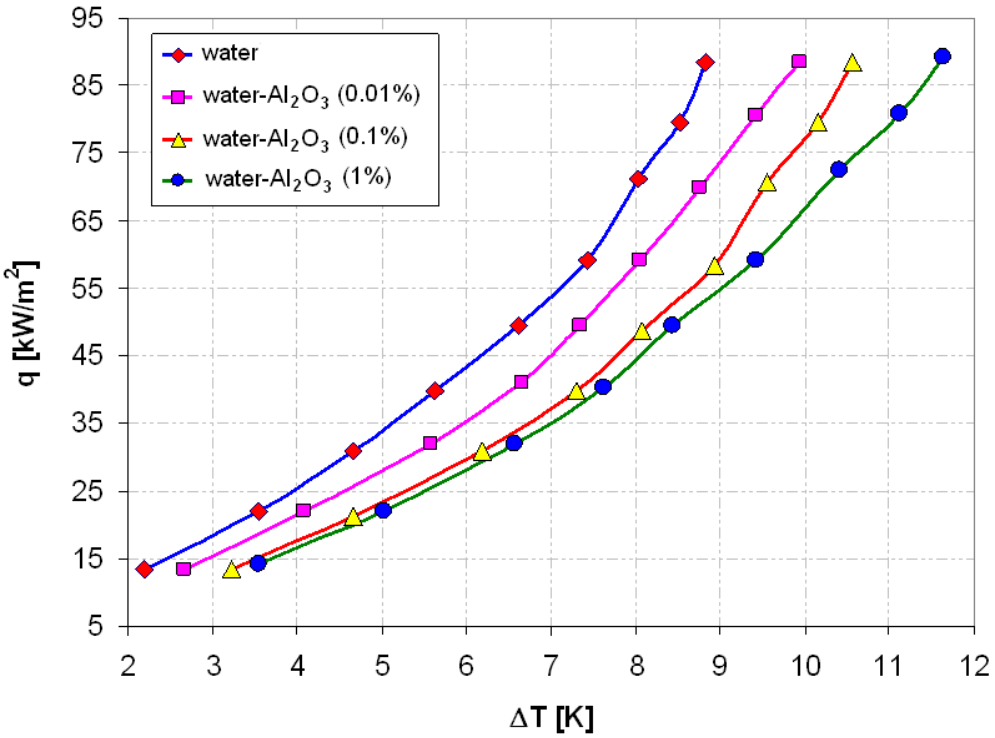

Figure 9 Boiling curves for water-Al_2O_3 nanofluid on porous coated tube at subatmospheric pressure (10 kPa)

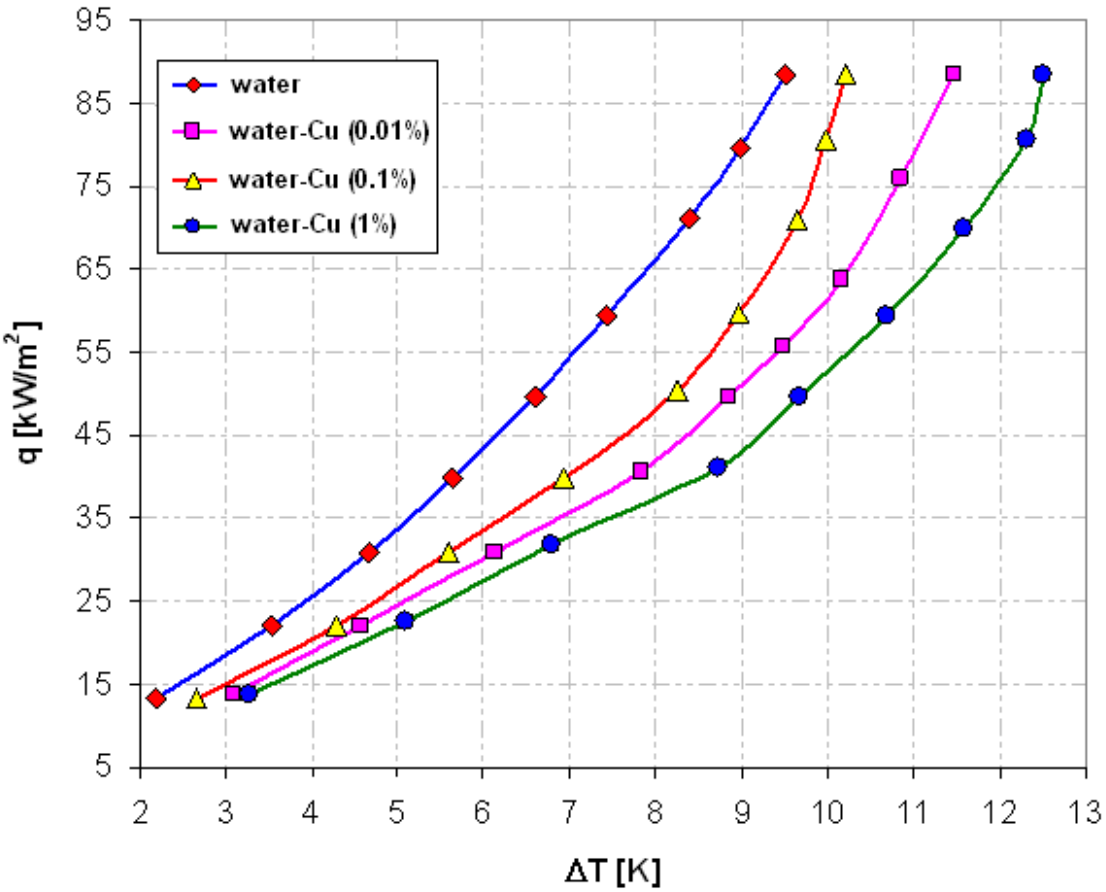

Figure 10 Boiling curves for water-Cu nanofluid on porous coated tube at subatmospheric pressure (10 kPa)

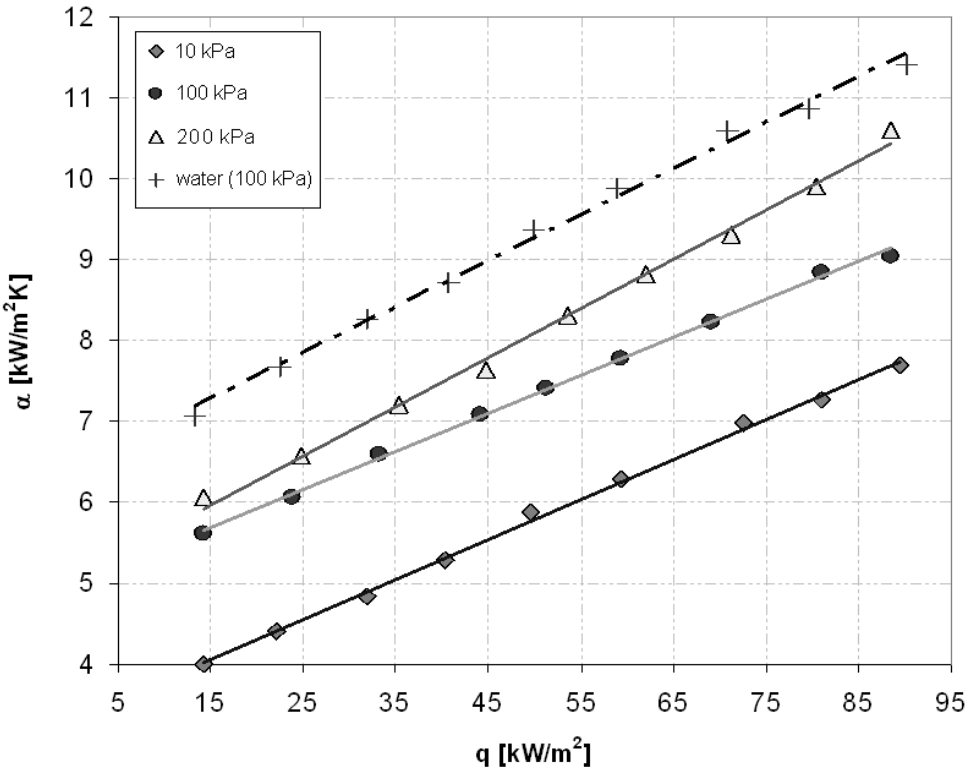

Figure 11 Heat transfer coefficient during boiling of water-Al_2O_3 nanofluid with 1% nanoparticle concentration on porous coated tube at different pressures

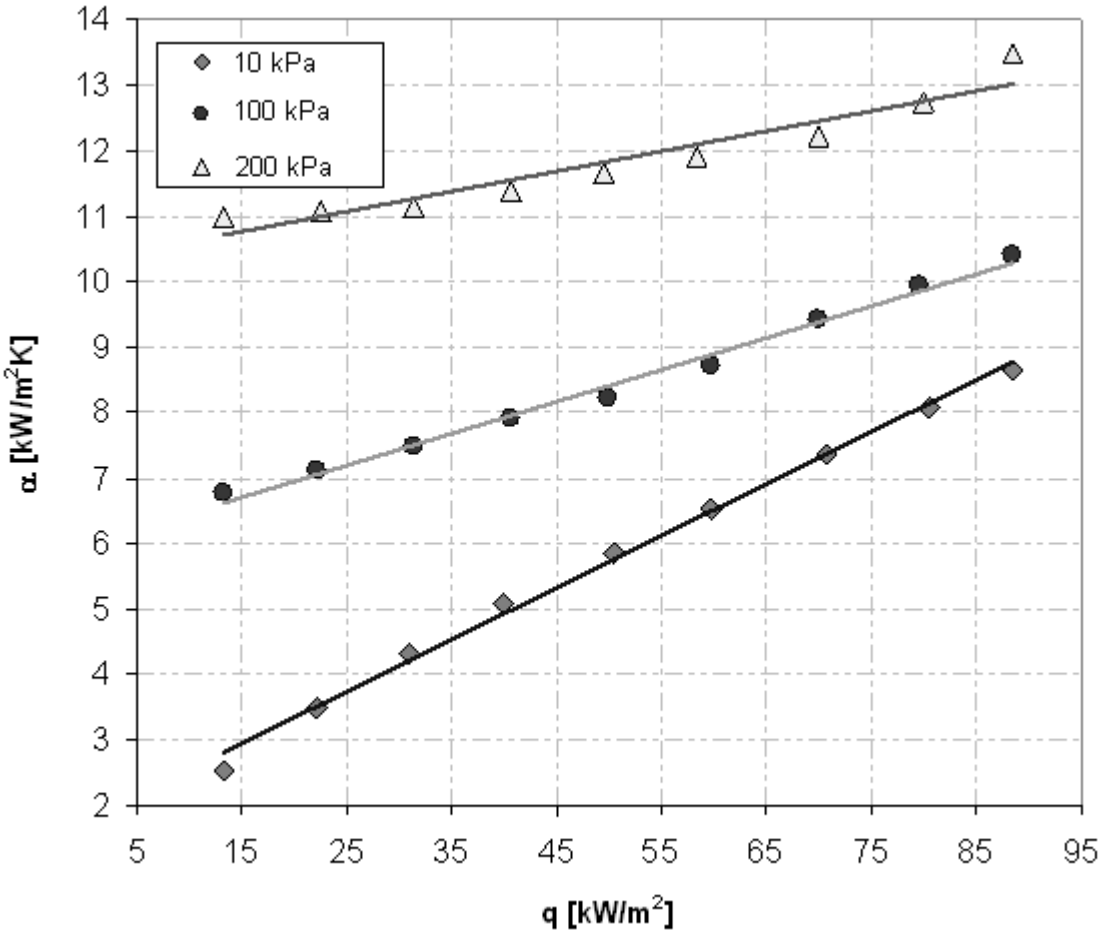

Figure 12 Heat transfer coefficient during boiling of water-Cu nanofluid with 0.1% nanoparticle concentration on porous coated tube at different operating pressures

a)

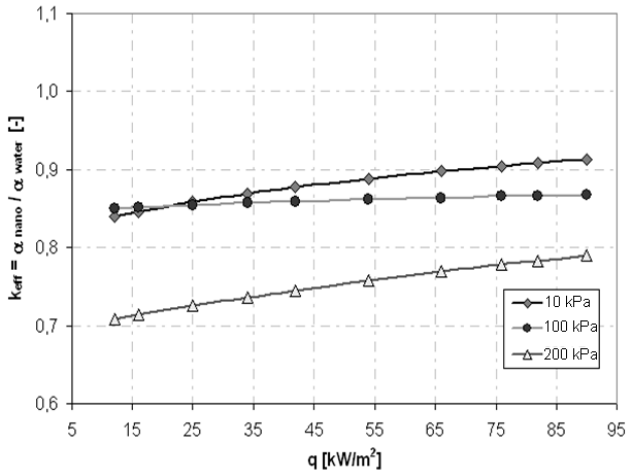

b)

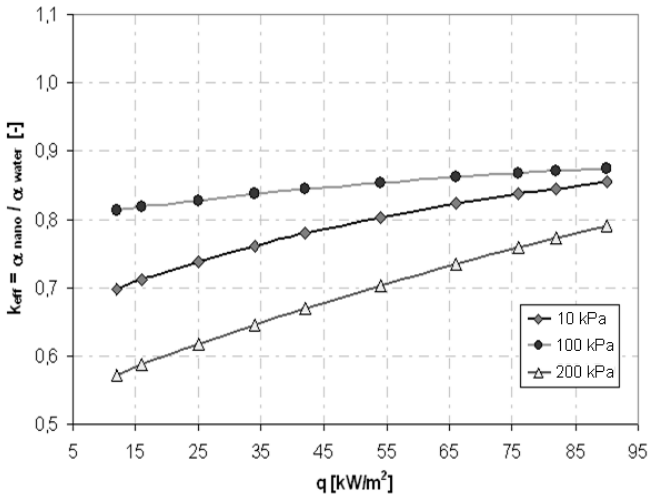

c)

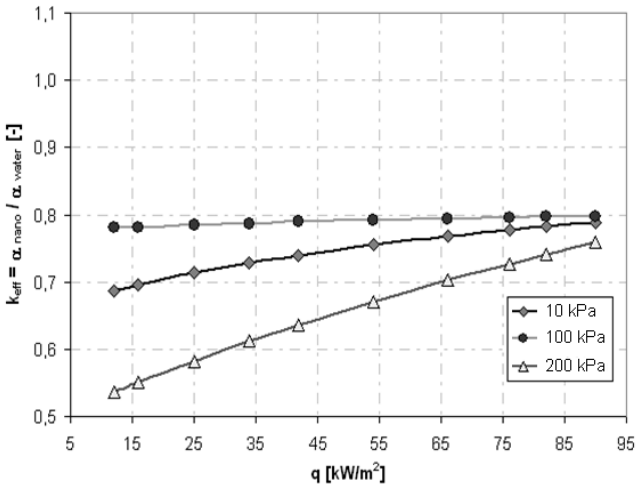

Figure 13 Enhancement factor for water-Al_2O_3 nanofluid during boiling on porous coated tube for various nanoparticle concentration: a) 0.01% b) 0.1%, c) 1% and different operating pressure

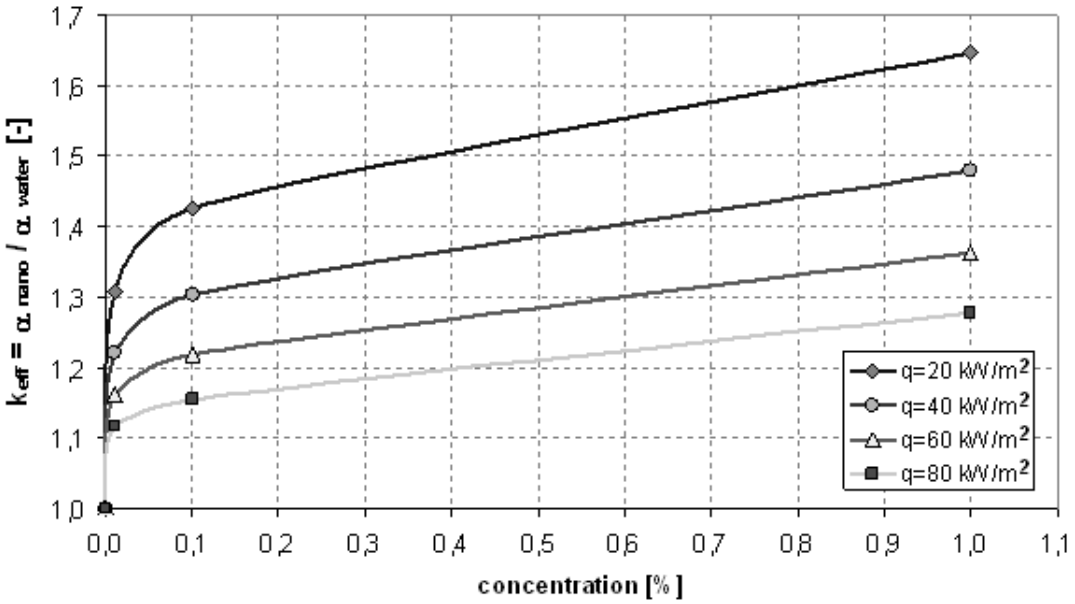

Figure 14 Enhancement factor for water-Al_2O_3 nanofluid during boiling on smooth stainless steel tube at atmospheric pressure versus nanoparticle concentration

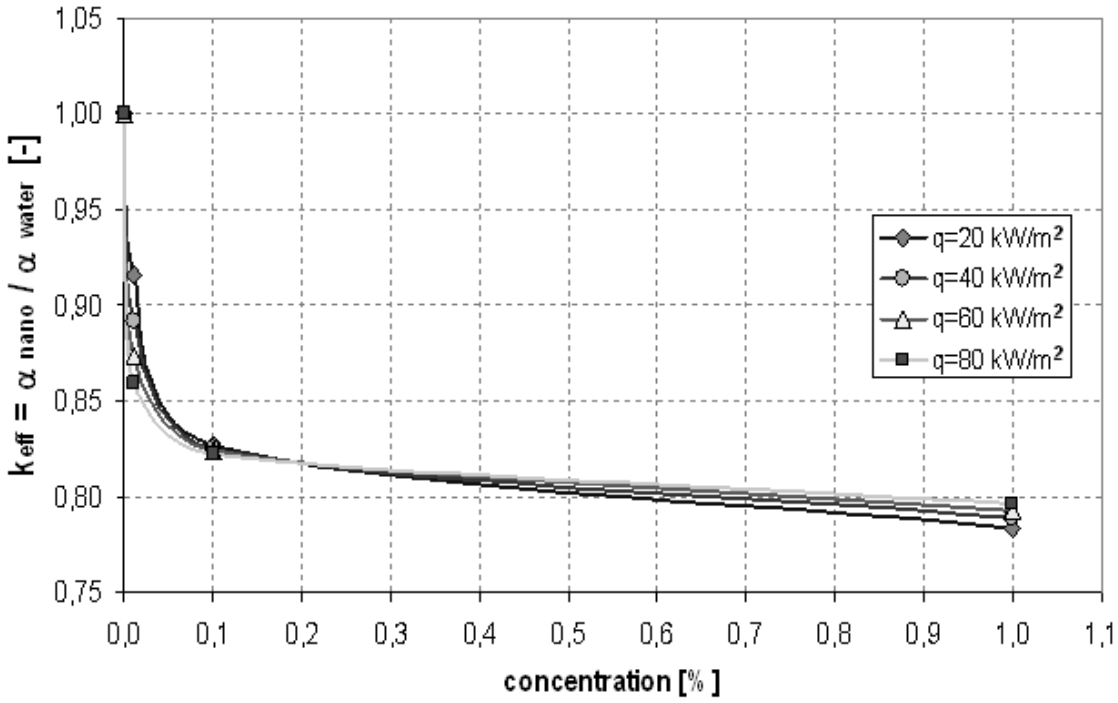

Figure 15 Enhancement factor for water-Al_2O_3 nanofluid during boiling on porous coated tube at atmospheric pressure versus nanoparticle concentration

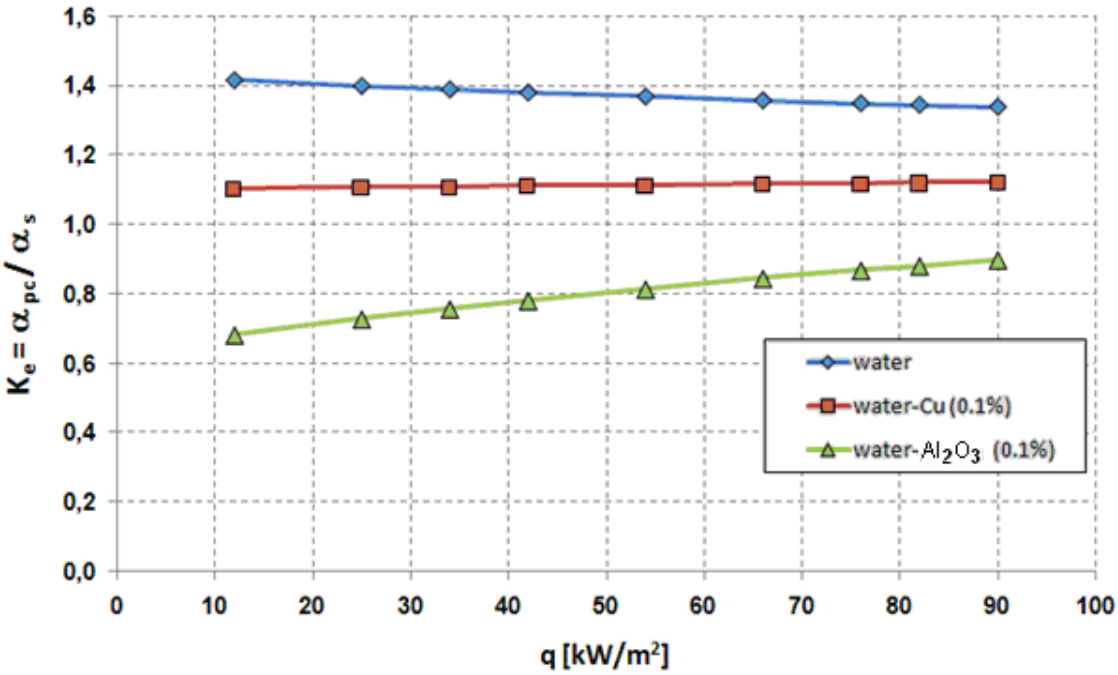

Figure 16 Ratio of the heat transfer coefficient for porous coated tube to the heat transfer coefficient for smooth tube during boiling of distilled water and nanofluids

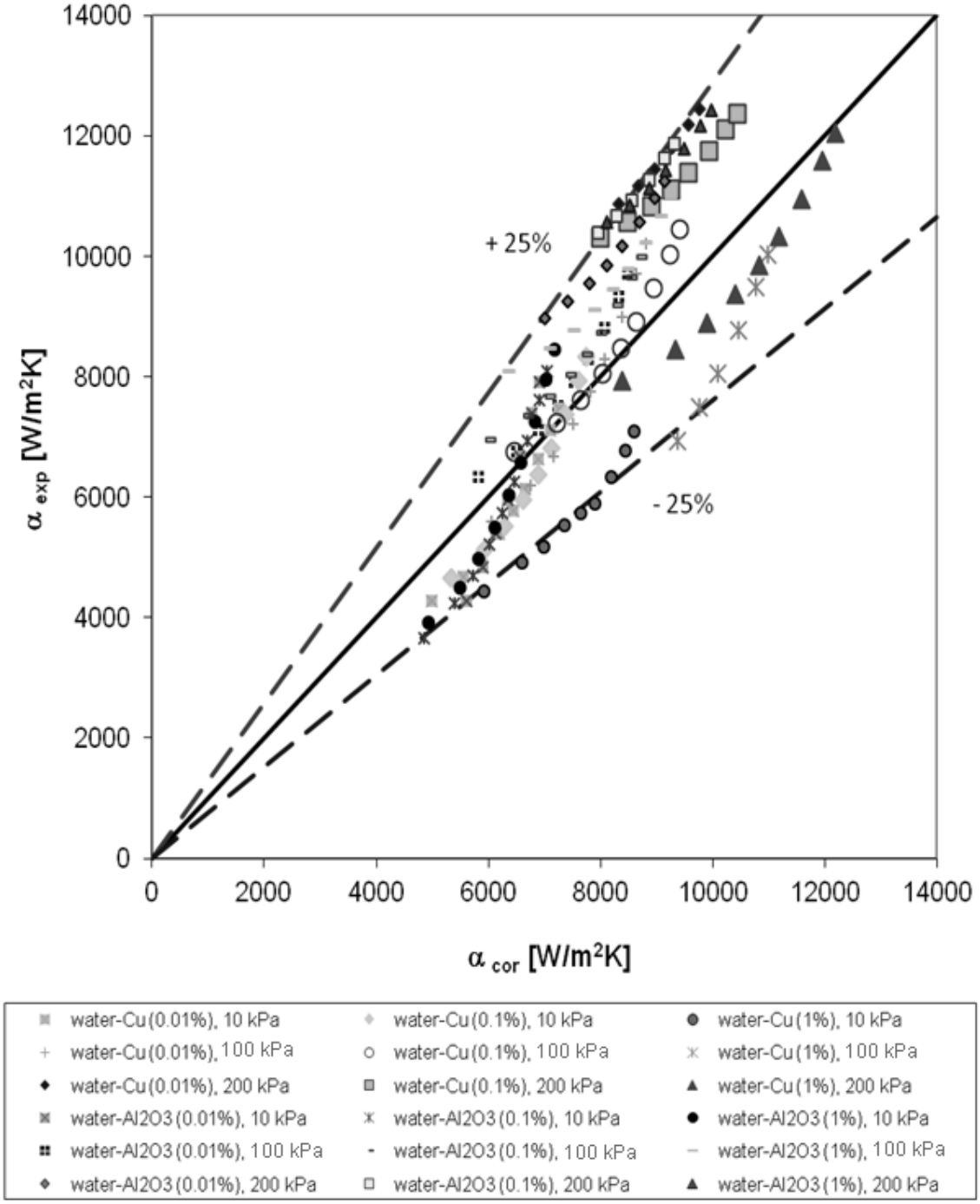

Figure 17 Comparison of the present data with the proposed correlation

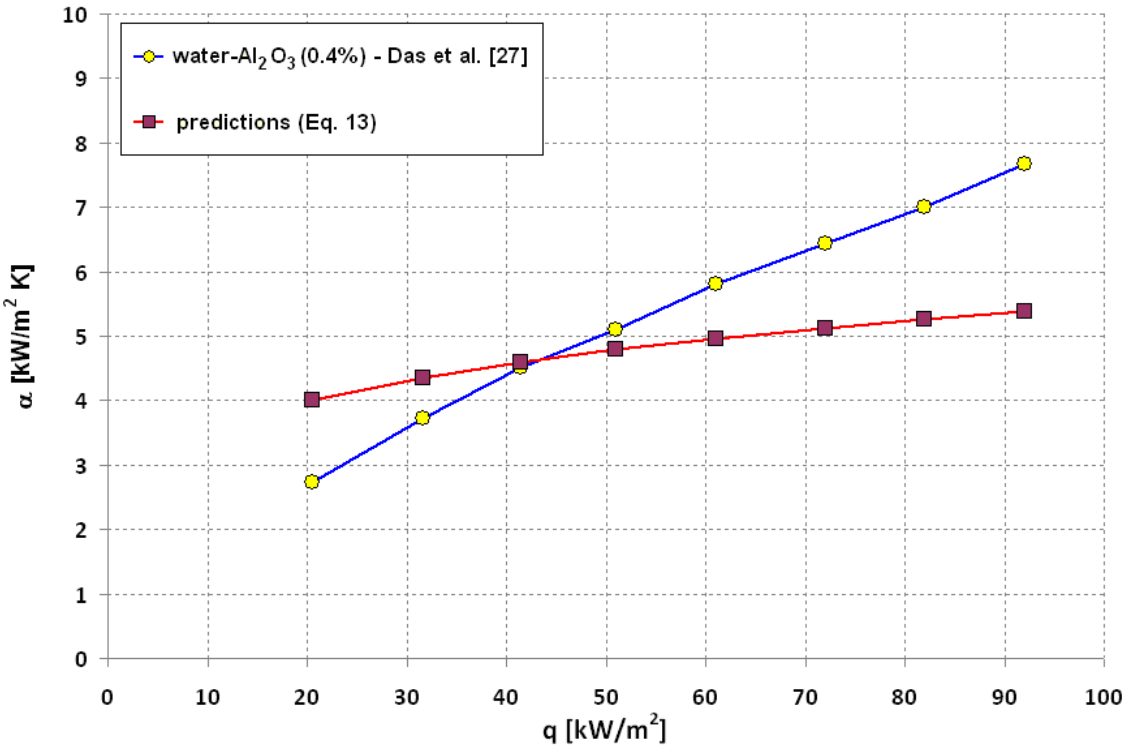

Figure 18 Comparison of predicted and experimental data obtained by Das et al. [27]

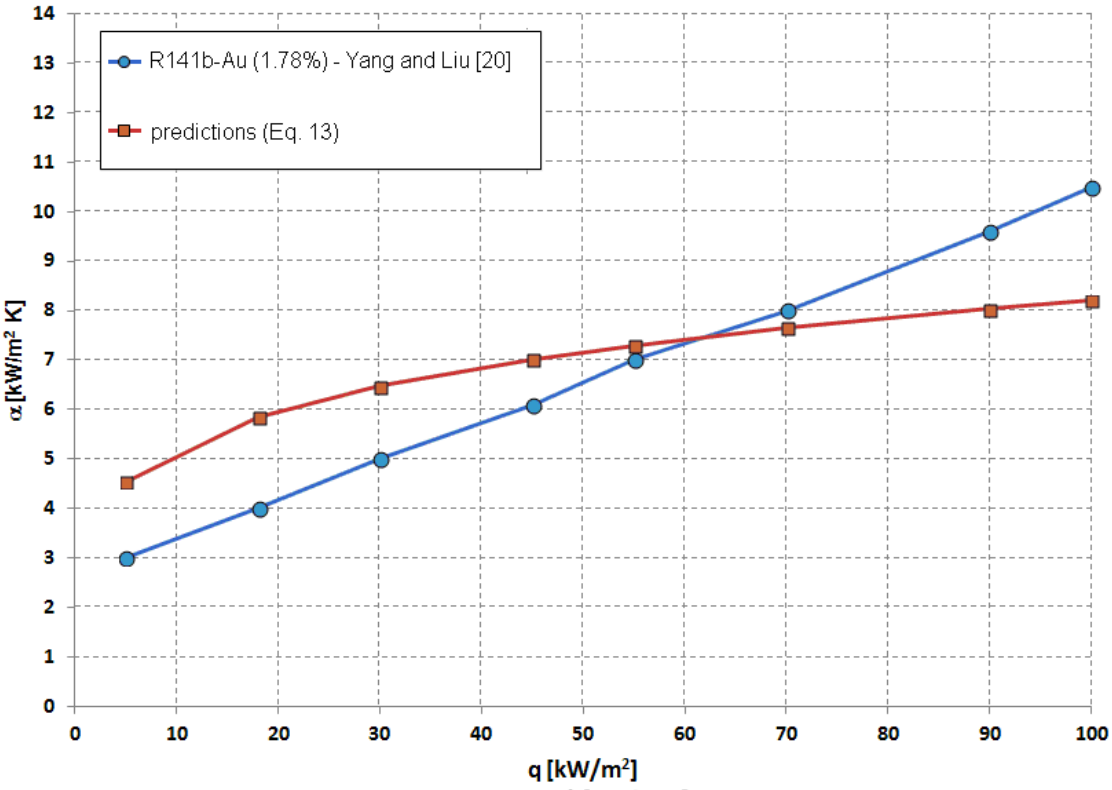

Figure 19 Comparison of predicted and experimental data obtained by Yang and Liu [20]

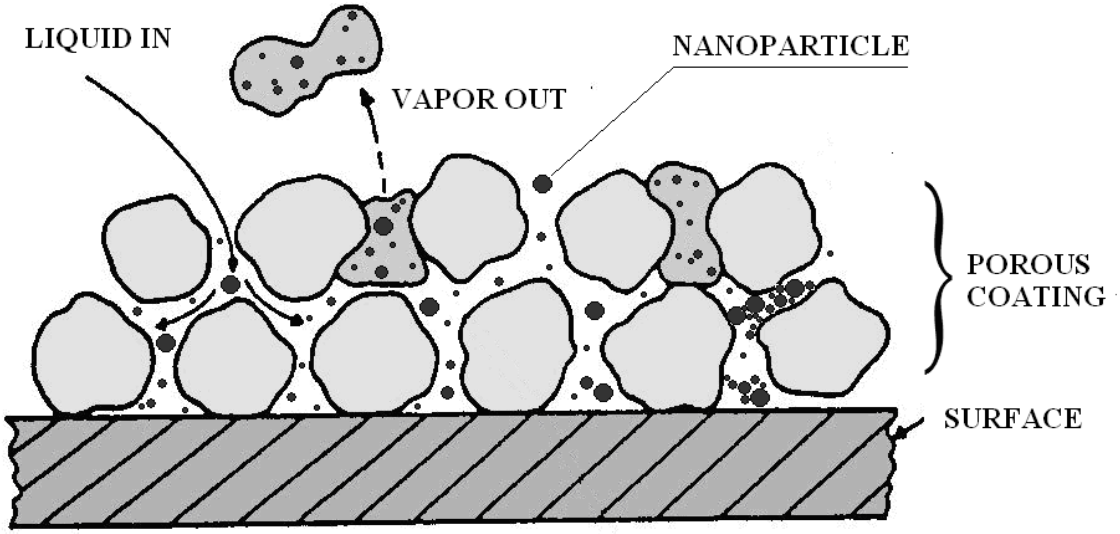

Figure 20 Nanoparticles behaviour during boiling on porous coating